CRYSTAL GROWTH & DESIGN

COMMUNICATION

pubs.acs.org/crystal

Cu_2O Template Strategy for the Synthesis of Structure-Definable Noble Metal Alloy Mesocages

Feng Hong, Shaodong Sun, Hongjun You, Shengchun Yang,* Jixiang Fang, Shengwu Guo, Zhimao Yang, Bingjun Ding, and Xiaoping Song*

School of Science, MOE Key Laboratory for Non-equilibrium Synthesis and Modulation of Condensed Matter, State Key Laboratory for Mechanical Behavior of Materials, Xi'an Jiaotong University, Shann Xi 710049, People's Republic of China

Supporting Information

ABSTRACT: We have demonstrated a novel strategy of synthesizing noble metal alloy mesocages *via* a Cu_2O template route. The efficiency of the current template route in producing alloy mesocages with various shapes (i.e., cube, octahedron, "star") was evaluated in diverse systems of Pt, Pd, as well as Pt/Pd. The current approach offered a facile and effective protocol for the synthesis of hollow noble metal mesocages (even nanocages).

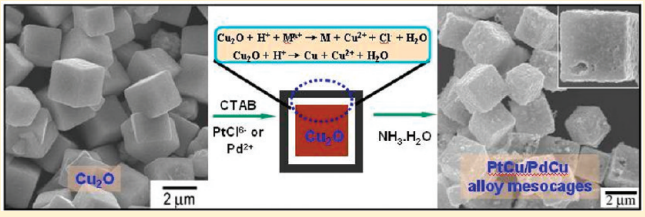

Noble metal meso-/nanocages represent a class of structures with high specific surface areas, rough surface, low densities, hollow interiors, and porous walls. Materials with such features are ideally suited to many advanced applications, for example, biomedical applications,[1] proton exchange membrane fuel cells,[2] and photocatalysis based on the photothermal effect.[3] Up to now, noble metal meso-/nanocages have been synthesized by several groups[2,4,5] using Ag polyhedrons, Co, Te, or Ni nanostructures as sacrificial templates via the galvanic replacement method or via selective removal of the core from the core/shell structures, e.g., Ag/Pt[2b] and Pd/silica.[6] Although many advances for the synthesis of hollow noble metal with controllable structures have been achieved, it still remains a challenge to investigate a facile, economical, and controllable approach for the synthesis of hollow noble metal meso-/nanostructures

In this study, we demonstrate a novel strategy to synthesize noble metal mesocages with various shapes and compositions using Cu_2O as sacrificial templates. As a p-type semiconductor with a band gap of 2.17 eV, Cu_2O has been considered as the promising material with potential applications in energy conversion, catalysis, and sensing.[7] Cu_2O crystals with well-defined sizes and shapes, such as cubic, octahedral, spherical, and even starlike shapes, have been widely reported,[8] which can be easily accessed and employed in the current template protocol. Furthermore, compared with the above widely reported templates, Cu_2O crystals have many special advantages, for example, easily controlled structures, cost saving, morphological multiformity, as well as large-scale production.[8c,d] It is noted that several hollow mesostructures, for example, CuS and Fe(OH)*x*, prepared using Cu_2O nanocrystals as sacrificial template, have been investigated in the systems of nonmetals or metal oxides.[9] However, the relative studies in noble metals are also an important issue in nanosynthesis.[10]

On account of the fact that the Cu_2O/Cu redox pair value of −0.36 V is much lower than that of a noble metal redox pair, such as $PtCl_6^{2-}/Pt$ 0.735 V and Pd^{2+}/Pd 0.987 V, therefore, the Cu_2O crystals can be potentially used as the candidate for the sacrificial templates for the synthesis of hollow noble metal nanostructures. The formation process of noble metal mesocages can be illustrated with Figure 1 and Figure S1 (in the Supporting Information, SI), which involves three steps: growth of Cu_2O crystals with different morphologies, the formation of Cu_2O/MCu (M = Pt, Pd) core/shell structures in H_2PtCl_6 or H_2PdCl_4 aqueous solution, and then the dissolution of the inner Cu_2O cores in ammonia solution.[9a] Besides octahedral Cu_2O crystal, cubic and starlike shapes are also chosen as the sacrificial templates.

The galvanic reaction between Cu_2O and metal ions in H_2PtCl_6 solution was performed immediately when the solution of H_2PtCl_6/H_2PdCl_4 was added into the mixture of Cu_2O and CTAB. The solution color changed from carmine to black after the addition of noble metal precursors, indicating the Pt or Pd ions were reduced quickly. In order to make the mesocages more unbreakable, the reaction was performed at 60 °C. This higher temperature could improve the aggregation and sintering of the attached nanoparticles, as shown in our previous work.[11] Herein, the concentration of H_2PtCl_6 solutions is 20 mM. After the reaction, the surface of the octahedrons became rough. Following the Cu_2O cores being dissolved in ammonia solution, PtCu mesocages with octahedral morphologies inherited from the Cu_2O templates (Figure 2a) are obtained (Figure 2b and c). As shown in the inset of Figure 2b, after the ultrasonic treatment in water, some partially broken octahedrons clearly show a

Received: February 8, 2011
Revised: June 23, 2011
Published: July 15, 2011

hollow interior. The TEM images of the PtCu mesocages also present an evidence for the formation of PtCu mesocages (Figure 2c). The thickness of the wall is estimated to be about 30 nm for PtCu mesocages. The selected area electron diffraction (SAED) patterns taken from a single octahedron show a fcc structure, and the PtCu shell is polycrystalline in nature. The five SAED rings can be approximately indexed to the {111}, {200}, {220}, {311}, and {222} lattice planes of Pt (inset in Figure 2c). High-resolution TEM micrographs show randomly oriented nanocrystals in the shell (Figure 2d), which is in agreement with the SAED results. The roughly measured grain size varies between 2 and 5 nm. The discrete spots in the FFT pattern (inset in Figure 2d) and lattice fringes indicate the crystallinity of the metal clusters. Notably, many voids can be observed on the shell, as shown by the arrows in Figure 2d. The distributions of the metallic elements in hollow mesocages can be analyzed by the X-ray element mapping and energy-dispersive X-ray spectroscopy (EDS) using HAABF-STEM. Figure 2c−e shows the representative STEM images of PtCu mesocages and corresponding Pt and Cu elemental maps. The distributions of both elements were readily detectable in the whole mesocages. Considering no copper diffraction peaks were observed and the obvious peak shifts in the XRD pattern (Figure 4) were found in PtCu mesocages, we think that the mesocages obtained through the reaction between Cu_2O and noble ions are alloy, rather than pure metals. The elemental compositions of the octahedron mesocages were measured by EDX and shown in SI Figure S2. The atomic ratios of Cu in Pt octahedron mesocages are around 16%.

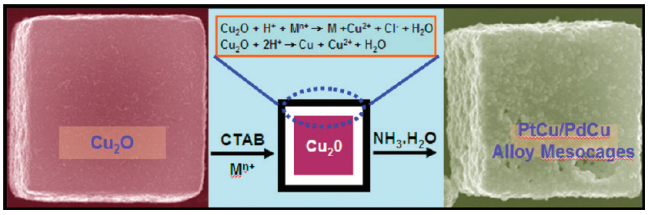

Figure 1. Schematic drawing of the formation of noble metal alloy mesocages.

Besides PtCu, PdCu octahedral mesocages can also be synthesized by similar methods, as shown in SI Figure S3, in which the atomic ratios of Cu are also around 12% (SI Figure S2b).

Compared with bimetallic nanostructures, recent studies suggest that the ternary alloys can have multifold increases in the electrocatalytic property because of their potentials in changing compositions, phases, and structure orders, which lead to their unique electronic, magnetic, and catalytic properties.[12] By using the same strategy, nonspherical hollow PtPdCu ternary mesocages can also be well produced. The procedure was the same as that of the hollow PtCu octahedron with half of H_2PtCl_6 replaced by H_2PdCl_4. Figure 3 shows SEM and TEM images of as synthesized PtPdCu octahedrons. Similar to the observations from PtCu and PdCu alloys, they display a rough surface (Figure 3a) and a hollow interior as shown by the inset in Figure 3a. The thickness of the wall is about 20 nm, a little thinner than that of PtCu and PdCu mesocages. The composition of the alloy octahedrons was studied by STEM mapping and EDX. Figure 3b−e show representative STEM images of hollow PtPdCu octahedrons and the corresponding Pt, Pd, and Cu elemental maps, from which one can see that both Pt, Pd, and Cu elements in the selected mesocages are of uniform distribution. The EDX data indicates that the atomic ratio of Cu is 9%, lower than the value measured from both PtCu and PdCu mesocages (See Figure S2c of the SI). The atomic ratio of Pd to Pt is 1.37:1, which is larger than the metallic ratio of 1:1 in initial additives. We consider that this result can be attributed to the fact that $PtCl_6^{2-}$ has a smaller value of the standard reduction potential than that of Pd^{2+} (0.735 V vs 0.987 V), and the Pd ion can be expected to be reduced more easily than Pt. Thus, Pd ions should generally be reduced first at the initial stages of reaction, resulting in a Pd-rich phase at the coating layer, which may act as a retardant for the reaction between remanent $PtCl_6^{2-}$ ions and solid Cu_2O. The TEM image also indicates their hollow character (Figure 3f). The SAED pattern on a mesocage reveals that the mesocages are polycrystalline, which can be further confirmed by the HRTEM image (Figure 3g) and the discrete spots in the FFT pattern. Two kinds of lattice spaces, as labeled in the image, are measured to be 0.22 and 0.191 nm, which are smaller than those of both pure Pt and Pd(111) plane (0.2245 and 0.2265) and

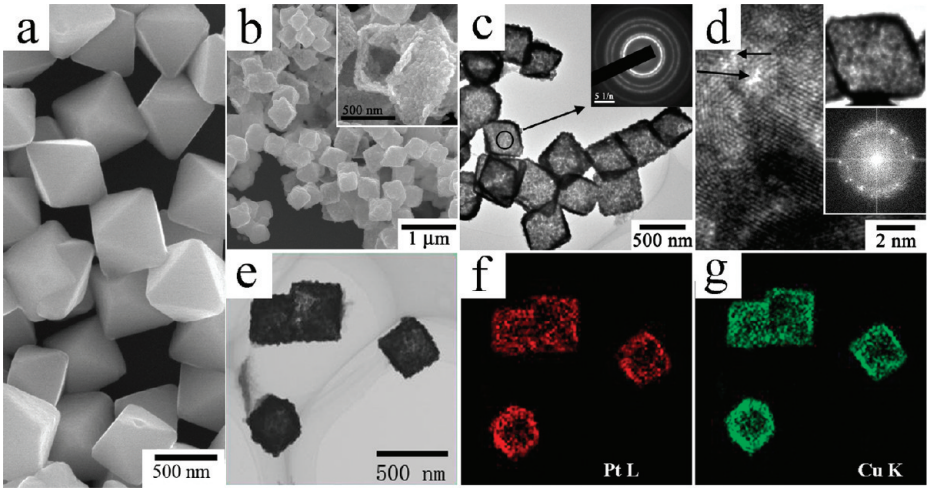

Figure 2. (a) SEM image of Cu_2O octahedrons; (b and c) SEM and TEM images of hollow PtCu octahedrons. The insert in part c shows the selective-area electron diffraction (SAED) pattern of the PtCu octahedron. (d) HRTEM image revealing that hollow PtCu octahedra were composed of small nanoparticles, and the insets show a single PtCu octahedron and the FFT pattern; (e) STEM images of PtCu octahedrons; (f and g) corresponding elemental maps for Pt and Cu in part e.

dx.doi.org/10.1021/cg2001893 |*Cryst. Growth Des.* 2011, 11, 3694–3697

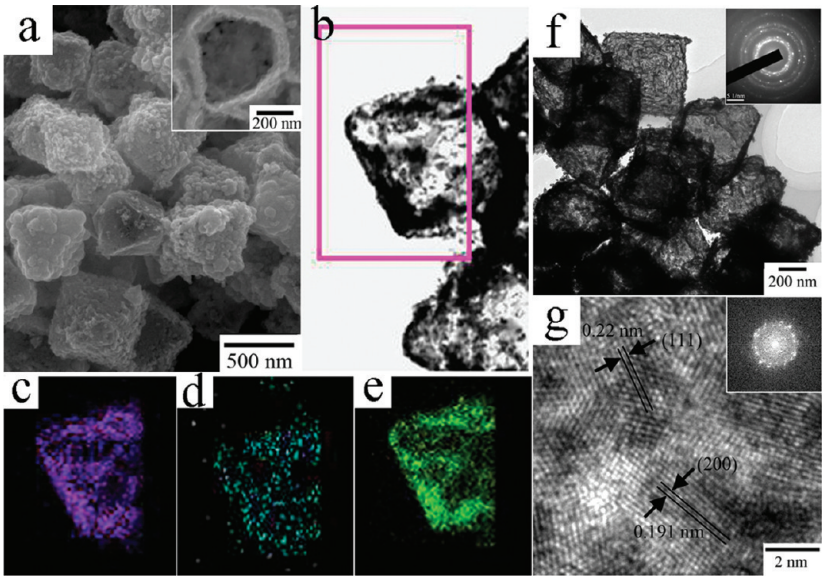

Figure 3. (a) SEM images of the hollow PtPdCu octahedron; (b−e) STEM images (b) and elemental maps (c−e) for Pt, Pd, and Cu, respectively; (f and g) TEM and HRTEM images of the hollow Pd octahedron. The insets of parts f and g show the SAED and FFT patterns of the PtPdCu octahedron.

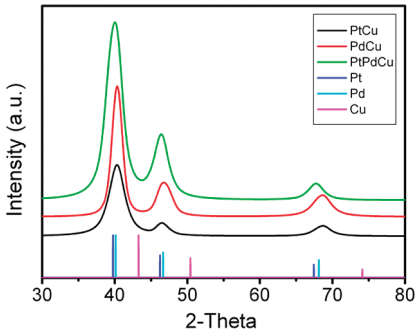

Figure 4. XRD patterns of as-prepared alloy mesocages for various alloy systems.

Pd(100) (0.1961 and 0.1945 nm), respectively, but larger than pure Cu(111) (0.2088 nm) and Cu(100) (0.1808 nm), implying the formation of ternary PtPdCu alloy.

X-ray diffraction patterns of the PtCu, PdCu, and PtPdCu alloy mesocages, as well as pure Pt, Pd, and Cu are compared in Figure 4. All three kinds of hollow materials could be indexed to (111), (200), and (220) diffractions, crystallizing in a similar disordered face-centered-cubic (fcc) structure, with the peak positions in between those of Pt/Pd and Cu metals. The reflection occurs in a 2θ around 40.3°, verging on the values of pure Pt(111), 39.76°, and Pd(111), 40.12°. Obviously, no other distinct diffraction peaks in all spectra than those of the peaks as mentioned above are observed, indicating the formation of alloys. Unlike the formation of ordered $Pt_{50}Bi_{50}$ and $Pt_{50}Pb_{50}$ alloy produced by using $NaBH_4$ as reducer at room temperature,[13] the formation of disordered alloys might be attributed to the fact that only a small quantity of copper atoms can be produced because of Cu/Cu^{2+} pairs (0.337 V) being much lower than that of $PtCl_6^{2-}/Pt$ (0.735 V) and Pd^{2+}/Pd (0.987 V) pairs in solution (SI Figure S2), leading to a low copper content in the final products. Therefore, the mesocages were formed as disordered alloy rather than ordered phase. At the same time, no diffraction

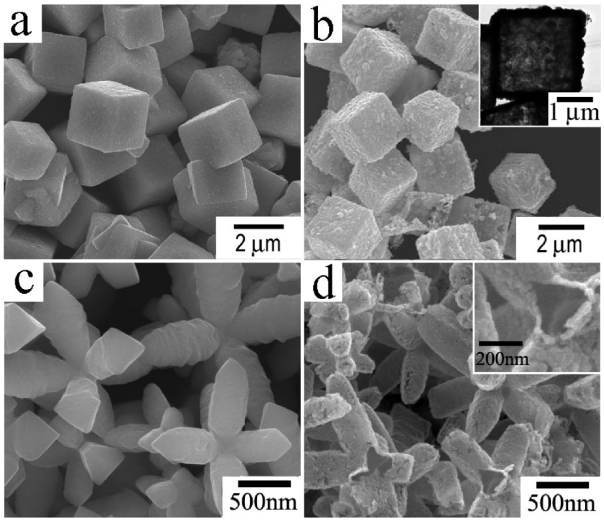

Figure 5. SEM images of cubic (a) and star-shaped (c) Cu_2O crystals; (b and d) SEM images of PdCu and PtCu hollow mesocages prepared by corresponding Cu_2O crystals. The insets in parts b and d show TEM images on hollow cubes and magnified images of some partially broken on the star-shaped structure.

peaks from Cu_2O appear, revealing that the remaining Cu_2O has been totally removed by ammonia solution. The lattice constant was calculated to be 3.895 Å and 3.864 Å for PtCu and PdCu on the basis of the PXRD data, respectively. These values correspond to the EDX results calculated according to Vegard's law and assuming a_{Pt} = 3.923 Å, a_{Pd} = 3.892 Å, and a_{Cu} = 3.619 Å (PCPDFWIN version 2.02).

The use of pregrown Cu_2O templates allows the morphologies of resultant hollow structures to be facilely designed. Cubic and star-shaped PdCu and PtCu mesocages with hollow interiors can also be synthesized by using the corresponding Cu_2O crystals (Figure 5) as the template. The SEM images of the final products were displayed in Figure 5b and d, indicating that the morphologies

of the Cu_2O cubes and star-shapes were kept very well after the galvanic reactions. The interior hollow structure could be observed through TEM images and partially broken on the surface from the insets of Figure 5b and d. The corresponding SAED patterns reveal that PdCu hollow cubes have a porous surface and present polycrystalline properties (SI Figure S4b). The compositions of these cubic mesocages are analyzed with the EDX spectrum, as shown in SI Figure S4a and S4b, and the atomic ratio between noble metal and Cu is 18.53:1 for PtCu and 10.4:1 for PdCu cubic mesocages, respectively. Additionally, by using this strategy, the spherical hollow Pt nanospheres with diameters less than 300 nm or larger than 4 μm can also be synthesized by using corresponding Cu_2O spheres as template (see SI Figure S5).

According to the above results, the coexistence of Cu can be attributed to the fact that the disproportionation reaction of Cu(I) in Cu_2O and the above galvanic reactions in the presence of H^+ can simultaneously produce metallic Cu and Pt (Pd), resulting in the formation of alloy nanoparticles. The reaction processes can be formulated as shown in Reactions 1−3. (See the SI for experimental details.)

$$2Cu_2O + 4H^+ + PtCl_6^{2-} \rightarrow Pt + 4Cu^{2+} + 6Cl^- + 2H_2O \quad (1)$$

$$Cu_2O + 2H^+ + Pd^{2+} \rightarrow Pd + 2Cu^{2+} + H_2O \quad (2)$$

$$Cu_2O + 2H^+ \rightarrow Cu + Cu^{2+} + H_2O \quad (3)$$

Although the reducing potential of Cu/Cu^{2+} pairs (0.337 V) is much lower than that of $PtCl_6^{2-}/Pt$ (0.735 V) and Pd^{2+}/Pd (0.987 V) pairs in solution, once the PtCu and PdCu alloy formed, the Cu atom might become hard to be oxided by Pt and Pd ions, which lead to a low ratio of Cu in the final products. However, the Cu can be removed by simply immersing the alloy mesocages into dilute HNO_3 solution, as shown in Figure S6 of the SI.

In summary, Cu_2O with controllable structures has been used as the sacrificial template for synthesis of nonsperical hollow metal mesocages. The template morphologies can be well inherited by the finial products. Using common metal oxide as templates is a facile, economical, and controllable approach to the synthesis of hollow meso-/nanocages. This work set the foundation for exploring a new strategy for the synthesis of hollow noble metal nanostructures

■ ASSOCIATED CONTENT

Supporting Information. Schematic drawing, EDX spectra, and SEM images of cubic and spherical Pt mesocages and Au and Ag nanocages. This material is available free of charge via the Internet at http://pubs.acs.org.

■ AUTHOR INFORMATION

Corresponding Author

*Tel: 86-29-82663034. Fax: 86-29-82665995. E-mail: ysch1209@mail.xjtu.edu.cn (S.C.Y.); xpsong@mail.xjtu.edu.cn (X.P.S.).

■ ACKNOWLEDGMENT

This work was supported by the National Basic Research Program of China (No. 2010CB635101), National Natural Science Foundation of China (No. 50901056 and 51071116), Doctoral Fund for New Teachers (No. 20090201120053), and Development Program of China (863 Program, No.2009AA03Z320). J.X.F. is supported by Tengfei Talent Project of Xi'an Jiaotong University.

■ REFERENCES

(1) (a) Chen, J. Y.; Glaus, C.; Laforest, R.; Zhang, Q.; Yang, M. X.; Gidding, M.; Welch, M. J.; Xia, Y. N. *Small* **2010**, *6*, 811–817. (b) Chen, J. Y.; Yang, M. X.; Zhang, Q. A.; Cho, E. C.; Cobley, C. M.; Kim, C.; Glaus, C.; L. Wang, H. V.; Welch, M. J.; Xia, Y. N. *Adv. Funct. Mater.* **2010**, *20*, 3684–3694. (c) Cheng, K.; Sun, S. H. *Nano Today* **2010**, *5*, 183–196.

(2) (a) Liang, H. P.; Zhang, H. M.; Hu, J. S.; Guo, Y. G.; Wan, L. J.; Bai, C. L. *Angew. Chem., Int. Ed.* **2004**, *43*, 1540–1543. (b) Peng, Z. M.; Wu, J. B.; Yang, H. *Chem. Mater.* **2010**, *22*, 1098–1106. (c) Peng, Z. M.; You, H. J.; Wu, J. B.; Yang, H. *Nano Lett.* **2010**, *10*, 1492–1496.

(3) (a) Cobley, C. M.; Au, L.; Chen, J. Y.; Xia, Y. N. *Expert Opin Drug Del* **2010**, *7*, 577–587. (b) Rycenga, M.; Wang, Z. P.; Gordon, E.; Cobley, C. M.; Schwartz, A. G.; Lo, C. S.; Xia, Y. N. *Angew. Chem., Int. Edit.* **2009**, *48*, 9924–9927.

(4) Sun, Y. G.; Xia, Y. N. *Science* **2002**, *298*, 2176–2179.

(5) (a) Zhang, G. X.; Sun, S. H.; Li, R. Y.; Sun, X. L. *Chem.—Eur. J.* **2010**, *16*, 10630–10634. (b) Seo, D.; Song, H. *J. Am. Chem. Soc.* **2009**, *131*, 18210–18211. (c) Huang, X. Q.; Zhang, H. H.; Guo, C. Y.; Zhou, Z. Y.; Zheng, N. F. *Angew. Chem., Int. Ed.* **2009**, *48*, 4808–4812. (d) Pasricha, Bala, R. T.; Biradar, A. V.; Umbarkar, S.; Sastry, M. *Small* **2009**, *5*, 1467–1473. (e) Lin, Z. H.; Chang, H. T. *Langmuir* **2008**, *24*, 365–367. (f) Lin, Z. H.; Lin, M. H.; Chang, H. T. *Chem.—Eur. J.* **2009**, *15*, 4656–4662. (g) Liang, H. W.; Liu, S.; Gong, J. Y.; Wang, S. B.; Wang, L.; Yu, S. H. *Adv. Mater.* **2009**, *21*, 1850–1854.

(6) Kim, S. W.; Kim, M.; Lee, W. Y.; Hyeon, T. *J. Am. Chem. Soc.* **2002**, *124*, 7642–7643.

(7) (a) Hara, M.; Kondo, T.; Komoda, M.; Ikeda, S.; Shinohara, K.; Tanaka, A.; Kondo, J. N.; Domen, K. *Chem. Commun.* **1998**, 357–358. (b) Zhang, J.; Liu, J.; Peng, Q.; Wang, X.; Li, Y. *Chem. Mater.* **2006**, *18*, 867–871. (c) Zhang, H.; Zhu, Q.; Zhang, Y.; Wang, Y.; Zhao, L.; Yu, B. *Adv. Funct. Mater.* **2007**, *17*, 2766–2771. (d) Yao, K. X.; Yin, X. M.; Wang, T. H.; Zeng, H. C. *J. Am. Chem. Soc.* **2010**, *132*, 6131–6144.

(8) (a) Wang, D. B.; Mo, M. S.; Yu, D. B.; Xu, L. Q.; Li, F. Q.; Qian, Y. T. *Cryst. Growth. Des.* **2003**, *3*, 717–720. (b) Sun, S. D.; Zhou, F. Y.; Wang, L. Q.; Song, X. P.; Yang, Z. M. *Cryst. Growth. Des.* **2010**, *10*, 541–547. (c) Kuo, C. H.; Huang, M. H. *Nano Today* **2010**, *5*, 106–116. (d) Chang, Y; Zeng, H. C. *Cryst. Growth. Des.* **2004**, *2*, 273–278.

(9) (a) Jiao, S. H.; Xu, L. F.; Jiang, K.; Xu, D. S. *Adv. Mater.* **2006**, *18*, 1174–1177. (b) Wang, Z. Y.; Luan, D. Y.; Li, C. M.; Su, F. B.; Madhavi, S.; Boey, F. Y. C.; Lou, X. W. *J. Am. Chem. Soc.* **2010**, *17*, 16271–16277.

(10) Fang, J. X.; Lebedkin, S.; Yang, S. C.; Hahn, H. *Chem. Commun.* 2011, Published on Web, DOI: 10.1039/C1CC10328H.

(11) Yang, S. C.; Wan, X. W.; Ji, Y. T.; Wang, L. Q.; Song, X. P.; Ding, B. J.; Yang, Z. M. *CrystEngComm* **2010**, *12*, 3291–3295.

(12) (a) Kowal, A.; Li, M.; Shao, M.; Sasaki, K.; Vukmirovic, M. B.; Zhang, J.; Marinkovic, N. S.; Liu, P.; Frenkel, A. I.; Adzic, R. R. *Nat. Mater.* **2009**, *8*, 325–330. (b) Geng, D. S.; Matsuki, D.; Wang, J. J.; Kawaguchi, T.; Sugimoto, W.; Takasu, Y. *J. Electrochem. Soc.* **2009**, *156*, B397–B402. (c) Sun, C. L.; Hsu, Y. K.; Lin, Y. G.; Chen, K. H.; Bock, C.; MacDougall, B.; Wu, X. H.; Chen, L. C. *J. Electrochem. Soc.* **2009**, *156*, B1249–B1252. (d) Wang, Z. B.; Zuo, P. J.; Yin, G. P. *Fuel Cells* **2009**, *9*, 106–113.

(13) Roychowdhury, C.; Matsumoto, F.; Zeldovich, V. B.; Warren, S. C.; Mutolo, P. F.; Ballesteros, M.; Wiesner, U.; Abruna, H. D.; DiSalvo, F. J. *Chem. Mater.* **2006**, *18*, 3365–3372.